



OPEN ACCESS

EDITED BY

Václav Ranc,
Palacký University, Czechia

REVIEWED BY

Oswaldo Andres Yáñez Osses,
University of the Americas, Chile
Renjith Thomas,
Mahatma Gandhi University, India

*CORRESPONDENCE

Minh Tho Nguyen,
minhtho.nguyen@vlu.edu.vn

SPECIALTY SECTION

This article was submitted to Analytical Chemistry, a section of the journal Frontiers in Chemistry

RECEIVED 21 September 2022

ACCEPTED 21 November 2022

PUBLISHED 05 December 2022

CITATION

Si NT, Nhat PV and Nguyen MT (2022), Binding mechanism and SERS spectra of 5-fluorouracil on gold clusters. *Front. Chem.* 10:1050423. doi: 10.3389/fchem.2022.1050423

COPYRIGHT

© 2022 Si, Nhat and Nguyen. This is an open-access article distributed under the terms of the [Creative Commons Attribution License \(CC BY\)](https://creativecommons.org/licenses/by/4.0/). The use, distribution or reproduction in other forums is permitted, provided the original author(s) and the copyright owner(s) are credited and that the original publication in this journal is cited, in accordance with accepted academic practice. No use, distribution or reproduction is permitted which does not comply with these terms.

Binding mechanism and SERS spectra of 5-fluorouracil on gold clusters

Nguyen Thanh Si ¹, Pham Vu Nhat ¹ and Minh Tho Nguyen ^{2,3*}

¹Department of Chemistry, Can Tho University, Can Tho City, Vietnam, ²Laboratory for Chemical Computation and Modeling, Institute for Computational Science and Artificial Intelligence, Van Lang University, Ho Chi Minh City, Vietnam, ³Faculty of Applied Technology, Van Lang University, Ho Chi Minh City, Vietnam

The adsorption behaviour of the 5-fluorouracil (5FU) on small gold clusters Au_N with N = 6, 8, 20 was evaluated by means of density functional theory using the PBE-D3 functional in combination with a mixed basis set, i.e. cc-pVDZ-PP for gold atoms and cc-pVTZ for non-metal elements. The binding energies between 5FU and gold clusters were determined in the range of 16–24 and 11–19 kcal/mol in gas-phase and aqueous media, respectively. The corresponding Gibbs energies were found to be around -7 to -10 kcal/mol in vacuum and significantly reduced to -1 to -6 kcal/mol in water solution, indicating that both the association and dissociation processes are likely spontaneous. An analysis on the charge density difference tends to confirm the existence of a charge transfer from the 5FU molecule to Au atoms. Analysis of the surface-enhanced Raman scattering (SERS) spectra of 5FU adsorbed on the Au surfaces shows that the stretching vibrations of N–H and C=O bonds play a major role in the SERS phenomenon. A mechanism for the drug releasing from the gold surfaces is also proposed. The process is triggered by either the low pH in cancerous tumors or the presence of cysteine residues in protein matrices.

KEYWORDS

5-fluorouracil, 5FU, SERS spectra, gold clusters, binding mechanism, binding energy, DFT

Introduction

The 5-fluorouracil molecule, denoted as 5FU in [Figure 1](#), which is commercialized under the trade name Adrucil, is one of the most widely used drugs in the cytotoxic chemotherapy to treat different cancers such as those of the colon, stomach, pancreas, breast, and esophagus ([Vodenkova et al., 2020](#)). The practical use of this drug has been well documented in both *in vivo* and *in vitro* studies ([Al-Jumayli et al., 2022](#); [Khodarahmi et al., 2022](#)), increasing the importance of the compound in the field of medicinal chemistry ([Li et al., 2021](#)). In view of its widespread use, it is necessary to focus on its increasing biocompatibility and reduction of its undesirable therapeutic effects. Some common side effects including loss of appetite, low blood cell count, hair loss,

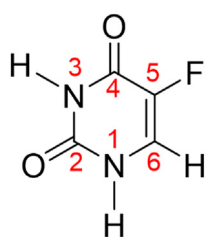


FIGURE 1
Chemical structure and atomic numbering of the drug molecule 5-fluorouracil (5FU).

inflammation of the mouth and skin, *etc.* Have been found (de Oliveira et al., 2021; Solhjoo et al., 2021). When topically used, it can cause skin irritation, especially during pregnancy (Oliveira et al., 2021). Therefore, it is extremely important to use the highly biocompatible, hydrophilic carriers to reduce such inherently damaged issues (Frydenberg et al., 2020; Wang et al., 2021). In addition to an improvement of the therapeutic efficacy of 5FU and a reduction of adverse events, it is also crucial to quickly detect its presence in a biological environment by a simple detection method (Yuksel et al., 2022).

Drug carriers play an important role in reaching the target area in the body as well as improving the therapeutic effect by adjustment of the optimal dose (Román et al., 2018; Zahed et al., 2018). While most polar drugs do not access cell membranes, nanomaterials can help solving this problem because of their high surface-to-volume ratio and low density. Furthermore, the small size, high stability and easily suitable surface modification properties of these nanomaterials also encourage their use as drug carriers (Al-Musawi et al., 2019; Horo et al., 2019).

For instance, the ability of the boron-fullerene B40 and its exohedral metallic derivatives (Au@B40 and Au4@B40) to carry 5FU was recently evaluated by DFT computations (Afarideh et al., 2018). Up to four Au atoms can be attached on the outer surface of the B40 cage at once to obtain the unique capability for delivering this molecule. Each Au atom has the potential to interact with one 5FU molecule when using only one B40 molecule. Due to the low binding energies and charge transfer, the 5FU drug can easily be detached from B40, Au@B40, and Au4@B40 at room temperature. The Ni-doped (8,0) boron nitride nanotube (Ni-BNNT) was employed as a 5FU adsorbent and sensor because it improved adsorption ability (up to -17 kcal/mol) against 5FU (Sanad et al., 2019). Additionally, a large charge transfer occurs between 5FU and Ni-BNNT (Aal, 2022). Due to their advantageous characteristics, the pure and encapsulated B36N36 nanoclusters have been recommended as potential new delivery systems and detectors for 5FU drugs. An important stage is the nature of the interactions between drugs and various nano-based materials that have been the subject of

numerous recent reports (Chen et al., 2022; Nguyen et al., 2022; Shakerzadeh et al., 2022; Yuksel et al., 2022).

Of the currently known nanomaterials such as carbon nanotubes (Minhas et al., 2021), boron nitride nanotubes (Kaur et al., 2019; Zarghami Dehaghani et al., 2021), chitin-chitosan (Sargazi-Avval et al., 2021), silica (Mirhaji et al., 2018), ninosome, the gold-based nanoparticles (Manzano and Vallet-Regí, 2020; Onishi et al., 2020; Siddique and Chow, 2020) are becoming attractive owing to their high biocompatibility, facile synthesis with many different sizes and shapes (Du et al., 2018; Khoshnevisan et al., 2018). These unique properties and applications in medicine have been discussed thoroughly in several recent reports (Elahi et al., 2018; Freitas de Freitas et al., 2018; Lee et al., 2020). In fact, gold nanoparticles have been approved as appropriate materials for many essential applications in biomedicine, biosensors and imaging (Bai et al., 2020; Bansal et al., 2020; Zhang et al., 2020). In this context, it is important to elucidate the interaction mechanism, as well as the binding nature, of the drug and gold nanoparticles (Sotnikov et al., 2019; Taghizadeh et al., 2019; Nhat et al., 2020a; Chen et al., 2021; Hang et al., 2021). It has been found that the interactions are mainly stabilized by a charge transfer from the electron-rich atoms of ligands to Au metals (Nhat et al., 2020b; Si et al., 2021). In some other cases, the gold atoms can act as a proton acceptor giving rise to nonconventional hydrogen bonds (Pakiari and Jamshidi, 2007; Nhat et al., 2020a). Nevertheless the interaction mechanism of gold nanoparticles is not well understood yet. From a methodological viewpoint, a question of interest is as to whether the particle surface could be modelled by some small-size clusters.

A majority of 80–85% of the administered 5FU drug is quickly converted to dihydroflourouracil during 5FU metabolism (Kryachko and Remacle, 2005). Furthermore, a tiny fraction (1–3%) of the drug given is transformed into fluorodeoxyuridine monophosphate and fluorouridine triphosphate, thereby inhibiting DNA synthesis and RNA processing. Urine excretes the remaining 12–19% of the unmetabolized 5FU form (Si et al., 2021). The concentration of 5FU in untreated wastewater was evaluated to be close to 18 ng/L (Tendwa et al., 2021) The ambient 5FU cytostatic drug concentration amounts to ~ 0.21 ng/L (Mazzuca et al., 2016). Numerous analytical methods (Rowney et al., 2009) have been used to detect 5-fluorouracil in blood sample, such as polarography (Franquet-Griell et al., 2015), amperometric (Dos Santos et al., 2022), photoluminescence (Ibrahim et al., 2018), high-performance liquid chromatography (Hanif et al., 2018; Liu et al., 2019), and gas chromatography-mass spectrometry (Gui et al., 2013). These techniques are effective, but they are costly due to the large testing costs, have limited throughput and take a long detection time because the sample must undergo complicated treatment procedures before analysis.

Therefore, it is now important to devise a quick, economic and convenient approach for the 5FU detection.

The surface-enhanced Raman scattering (SERS) phenomenon occurs when a Raman active molecule is adsorbed on the surface of a nanoparticle, considerably enhancing its Raman intensities (Schlücker, 2014). The electromagnetic (EM) and charge transfer (CT) mechanisms emerge now as the two main explanations for the enhancing mechanism of SERS. According to the EM approach, the enhancement is mostly due to interactions between molecules and the massive surface resonance plasmons that an incoming laser causes to form on the substrate's surface (Mullot et al., 2009). Following the CT approach, the increase also involves a significant charge transfer as during the associated electronic resonance transition between the molecules and the substrate (Schlücker, 2014). For the detection of a single molecule, the SERS technique appears to be a highly sensitive analytical technique because of its high enhancement efficiency (Weiss and Haran, 2001).

In this context, we set out to carry out in present study quantum chemical calculations with the aim to evaluate the binding mechanism between gold nanoparticles and the 5FU molecule by using the gold Au_N clusters with $N = 6, 8, 20$ as models for the gold surfaces. In addition, the surface enhanced Raman scattering (SERS) mechanism and the applicability of gold nanoparticles for detection of the 5FU molecule are also elucidated.

Computational methods

All electronic structure calculations in this study are performed using density functional theory (DFT) with the PBE-D3 functional (Perdew et al., 1996; Grimme et al., 2010) including the dispersion correction (D3) in conjunction with the effective core potential (ECP) cc-pVDZ-PP (Peterson, 2003) for gold atoms and the cc-pVTZ basis set for other atoms using the Gaussian 16 package (Frisch et al., 2019). In the cc-pVDZ-PP basis set, the inner electrons along with the nucleus are considered as an inert core, and those on $5s$, $5p$, $5d$, and $6s$ orbitals of the Au atom are taken as valence electrons. The interaction between valence electrons and inert core is included in the pseudopotential which also takes care of the relativistic effects of the heavy gold atoms. This allows us to reduce greatly the number of electrons to be treated, and thereby computing times, but still describe properly the interactions between gold atoms and biomolecules (Nhat et al., 2020a; Nhat et al., 2020b). In addition, the Integral Equation Formalism-Polarizable Continuum Model (IEF-PCM) (Tomasi et al., 2005) is employed to investigate the effects of aqueous solvents. The density of states (DOS) are simulated by using the GaussSum program (O'boyle et al., 2008). The charge density difference (CDD) maps and energy decomposition analyses are obtained by using the Multiwfn 3.8 software (Lu and Chen, 2012).

The binding energies (E_b) is simply defined as the energy difference between those of the Au_N -5FU complexes with respect to the free 5FU drug molecule and the Au_N ($N = 6, 8, 20$) species:

$$E_b = E_{Au_N-5FU} - (E_{Au_N} + E_{5FU})$$

where E_{Au_N-5FU} is the total energy of the E_{Au_N-5FU} complexes, E_{Au_N} and E_{5FU} the total energies of Au_N ($N = 6, 8, 20$) clusters and 5FU drug, respectively. Thus, a negative value of E_b corresponds to an exothermic adsorption.

The Gibbs free energy of the interaction are calculated as follow:

$$\Delta G^0 = (E + G_{corr})_{Au_N-5FU} - [(E + G_{corr})_{Au_N} + (E + G_{corr})_{5FU}]$$

where $(E + G_{corr})$ is the sum of electronic and thermal free energies.

The energies of frontier states such as HOMO and LUMO, and the derivative HOMO-LUMO band gap (E_g) are also computed to examine the electronic responses during adsorptions. The E_g is a useful factor for determining the kinetic reactivity of materials (Hadipour et al., 2015), and its change upon the adsorption process can be used to evaluate the sensitivity of absorption.

Results and discussion

Structures of 5FU drug and gold clusters

Several theoretical and experimental studies (Scanlan and Hillier, 1984; Hadipour et al., 2015; Wieleńska et al., 2019) have previously been conducted to determine the chemical structure of 5FU drug and at least eight different tautomers have been located (cf. Figure 2). Accordingly, the molecule exhibits a planar structure, containing a six-membered N-heterocyclic ring (pyrimidine ring) with a fluorine substituent at the C5 position. This modification process is completely similar to that of DNA bases as a result of the hydrogen transfer within oxygen and nitrogen atoms (Pascu et al., 2005; Markova et al., 2010).

Generally, the proton transfer in the 5FU molecule results in eight possible tautomers (Figure 2), including one di-keto (5FU), four keto-enols (5FU_1, 5FU_2, 5FU_7 and 5FU_8), and three di-enols (5FU_3, 5FU_4 and 5FU_5). The two rotational conformations (5FU_7 and 5FU_8) are also found upon rotation of the O-H group around the C-O group (5FU_1, 5FU_2). This is similar to that of 5FU_4 and 5FU_5 isomers. At the PBE-D3/cc-pVTZ level, the 5FU structure is 9–16 kcal/mol more stable than its tautomeric forms (gas-phase values). Such an energy gap is reduced to 1–8 kcal/mol in the aqueous solution. These computed results are fully consistent with both theoretical and experimental results previously reported (Scanlan and Hillier, 1984; Markova et al., 2010). The predicted distance of

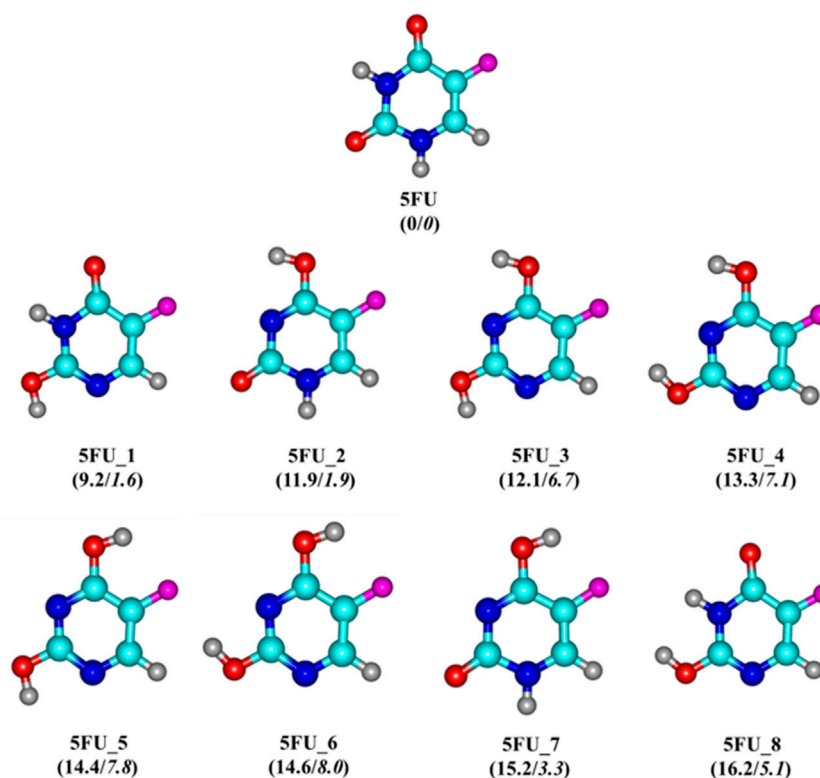


FIGURE 2

Optimized structures of 5FU and its tautomers. Values (kcal/mol) given in parentheses represent relative energies of 5FU tautomers at the PBE-D3/cc-pVTZ + ZPE level in vacuum/water solution with respect to 5FU.

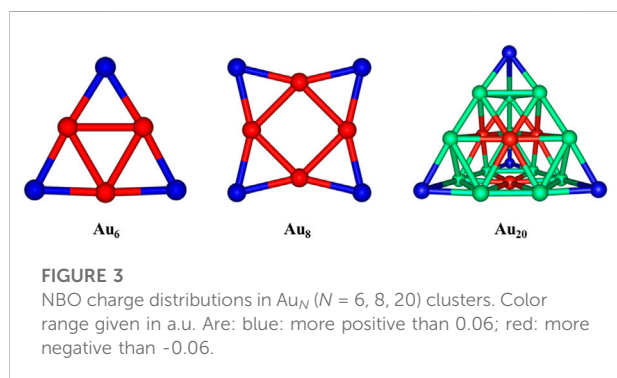


FIGURE 3

NBO charge distributions in Au_N ($N = 6, 8, 20$) clusters. Color range given in a.u. Are: blue: more positive than 0.06; red: more negative than -0.06.

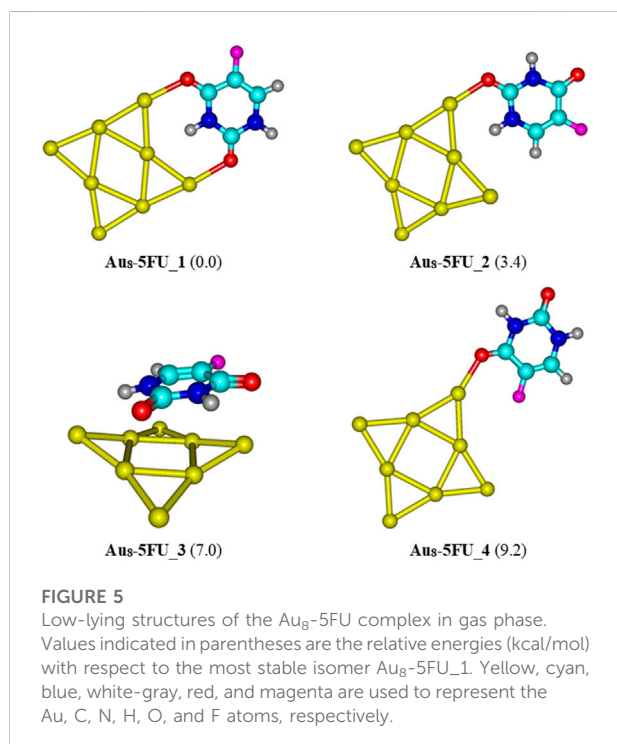
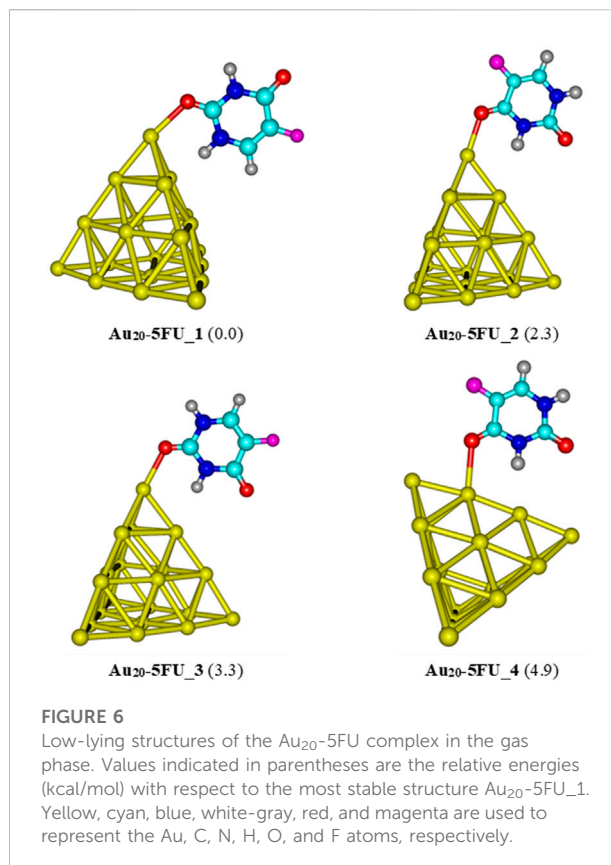
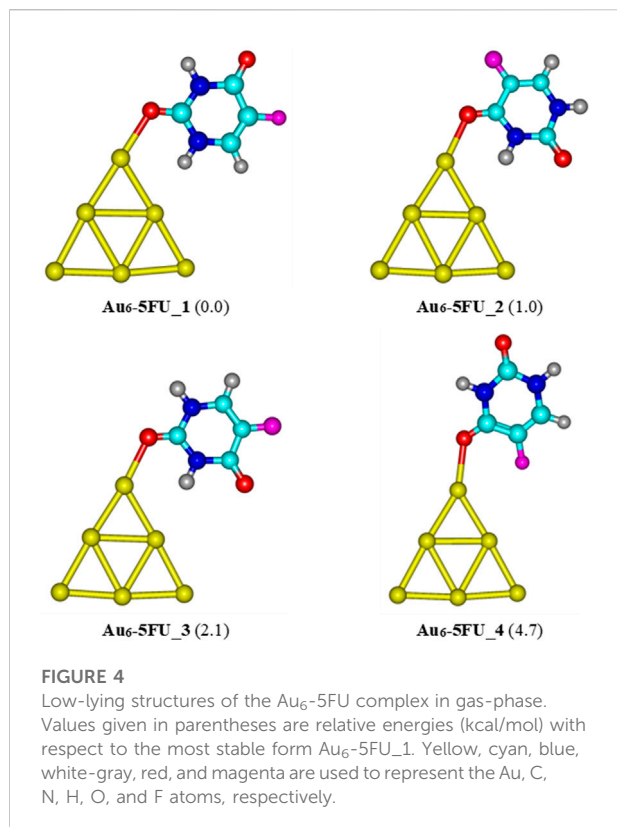
the C–F bond is 1.341 Å, which is comparable to the experimental value of 1.348 Å (Rastogi et al., 2000). The bond lengths of C2 = O and C4 = O are computed to be 1.220 and 1.221 Å, respectively, being somewhat longer than the experimental values of 1.212 and 1.211 Å (Rastogi and Palafox, 2011).

As reported earlier, the Au_6 and Au_8 clusters have planar structures, while the Au_{20} cluster gas prefers a pyramidal shape in their ground states (Rastogi and Palafox, 2011). To determine the

favoured binding sites between the gold clusters and the 5FU molecule, an analysis of NBO charge distribution (Rastogi et al., 2000) is first carried out and presented in Figure 3. The corner Au atoms (blue color) are found to bear a more positive charge than others (red color). According to previous studies (Nhat et al., 2017; Nhat et al., 2020b), the 5FU molecule is expected to interact with gold clusters by anchoring its electron-rich sites on the positively charged atoms of gold surfaces. In addition, the binding is in part stabilized due to the formation of some nonconventional X–H...Au hydrogen bonds. To evaluate the dynamic stability of the gold cluste-5FU complexes we carry out Born-Oppenheimer molecular dynamics simulations for Au_6 -5FU and Au_8 -5FU systems at 300 K. Simulation results that are collected in Figure S3 (SI file), show the connectivity between atoms in these systems remains unchanged during the simulation time, indicating that they are dynamically stable.

Absorption of 5FU drug on gold cluster surface: Structures and energies

Four structures of Au_N -5FU ($N = 6, 8, 20$) complexes obtained at the PBE-D3/cc-pVTZ/cc-pVDZ-PP level are



displayed in Figure 4–6. Accordingly, the most stable structure of Au₆-5FU complexes contains an Au–O bond constructed by anchoring the oxygen atom of the C2 = O group on the corner of Au₆. This structure is almost planar with an Au–O bond length of 2.317 Å. The oxygen atom of the C4 = O group is the next preferred site for Au₆ attack, resulting in the Au₆-5FU₂ complex. This form is ~1.0 kcal/mol less stable than Au₆-5FU₁. The two remaining structures, namely Au₆-5FU₃ and Au₆-5FU₄, that can be considered as rotational isomers of Au₆-5FU₁ and Au₆-5FU₂, respectively, are lying around 2–5 kcal/mol above. A perpendicular anchor type between the Au₆ cluster and the 5FU molecule is not found.

As in Au₆-5FU, the oxygen atom of the C2 = O and C4 = O carbonyl groups is also the most preferred site for 5FU binding to Au₈ (Figure 5). The lowest-energy Au₈-5FU₁ has a binding energy of –24 kcal/mol, as compared to a corresponding value of –17 kcal/mol obtained for Au₆-5FU₁ (Figure 4). This structure is stabilized mainly due to interaction of 2 C=O bonds with the Au₈ cluster. The next stable complex Au₈-5FU₂ is ~3.4 kcal/mol higher in energy than Au₈-5FU₁. Noticably, we find a new type of adsorption, i.e. Au₈-5FU₃, in which the 5FU molecule is lying parallelly on the gold surface. However, such interaction induces a slight change in geometry of

TABLE 1 Relative energy (RE), binding energy (E_b) and Gibbs free energy (ΔG) for the 5FU adsorption on gold clusters Au_N with $N = 6, 8, 20$ in their optimized complexes (PBE-D3/cc-pVTZ/cc-pVDZ-PP, kcal/mol).

Structure	Re		E_b		ΔG	
	In gas phase	In water	In gas phase	In water	In gas phase	In water
Au6-5FU_1	0.0	0.8	-16.8	-12.6	-6.5	-3.0
Au6-5FU_2	1.0	0.0	-15.8	-13.4	-5.7	-2.1
Au6-5FU_3	2.1	0.6	-14.7	-12.8	-4.8	0.1
Au6-5FU_4	4.7	2.6	-12.1	-10.7	-4.0	0.3
Au8-5FU_1	0.0	0.0	-23.5	-19.1	-9.7	-6.3
Au8-5FU_2	3.4	0.0	-20.1	-15.3	-8.2	-3.6
Au8-5FU_3	7.0	2.9	-16.4	-16.2	-4.9	-2.0
Au8-5FU_4	9.2	6.1	-14.3	-13.0	-5.1	-5.2
Au20-5FU_1	0.0	1.8	-16.8	-11.3	-7.5	-1.5
Au20-5FU_2	2.3	0.7	-14.5	-12.4	-3.5	-1.9
Au20-5FU_3	3.3	0.0	-13.5	-13.1	-2.5	-2.8
Au20-5FU_4	4.9	2.4	-11.8	-10.7	-1.6	0.0

Au_8 cluster. Similar to the Au_6 -5FU system, the $C4 = O$ group is not a preferred site for binding to the gold atoms. Indeed, this binding pattern (Au_8 -5FU_4) has a relative energy of ~ 9 kcal/mol higher than the most stable form.

For the interaction between the pyramidal Au_{20} and 5FU, four stable structures are identified and presented in Figure 6. The most stable form Au_{20} -5FU_1 has a binding energy of around -17 kcal/mol. The next stable complex Au_{20} -5FU_2 is formed by anchoring the O atom of the $C4 = O$ group on a corner of Au_{20} is computed to be ~ 2.3 kcal/mol less stable than Au_{20} -5FU_1. The structure Au_{20} -5FU_3 is also rather stable as located at ~ 3 kcal/mol above Au_{20} -5FU_1 and is basically considered as a rotational isomer of the latter. On the contrary, the resulting complexes that are formed by adsorption of 5FU on an Au atom at the edge of the Au_{20} cluster are much less stable, being ~ 5 kcal/mol higher in energy.

Table 1 presents the calculated binding energy (E_b) and Gibbs free energy (ΔG) for the 5FU adsorption on gold clusters obtained at the PBE-D3/cc-pVTZ/cc-pVDZ-PP level. The adsorption processes are exothermic indicating all stabilizing interactions. However, due to entropic effects, i.e. entropy is decreased during the adsorption, the Gibbs free energies turn out to be less negative as compared to corresponding binding enthalpies. In particular, the higher reactivity toward the 5FU molecules of Au_8 in comparison with Au_6 and Au_{20} clusters correlates with its smaller HOMO-LUMO gap and lower stability (Nhat et al., 2020a).

When including the influence of an aqueous solvent, both E_b and ΔG values become less negative than those computed in vacuum. The numerical data obtained for interactions of 5FU molecule and Au_N ($N = 6, 8, 20$) clusters in a water environment presented in Table 1 show that the Au_8 cluster also has the highest affinity with the 5FU molecule.

In the most stable complexes Au_N -5FU_1 ($N = 6, 8, 20$), the bond lengths of Au-O amount to 2.317, 2.359 (2.417), and 2.404 Å in gas phase and 2.329, 2.337 (2.370), and 2.397 Å in water, respectively. Thus it can be seen that the bidentate formation of Au-O bonds in Au_8 -5FU_1 correlates well with its largest bonding energy. Overall, the bond lengths are predicted to be slightly longer than the sum of the covalent radii of oxygen (0.73 Å) and gold (1.44 Å) atoms (Pakiari and Jamshidi, 2007).

Electronic properties of frontier orbitals

For deeper insights into the interaction mechanisms, we now consider the energies of frontier orbitals, namely the HOMO and LUMO, in both isolated components and resulting products. The change of the HOMO-LUMO energy gap (ΔE_g) of gold clusters during the 5FU adsorption is computed using the following equation:

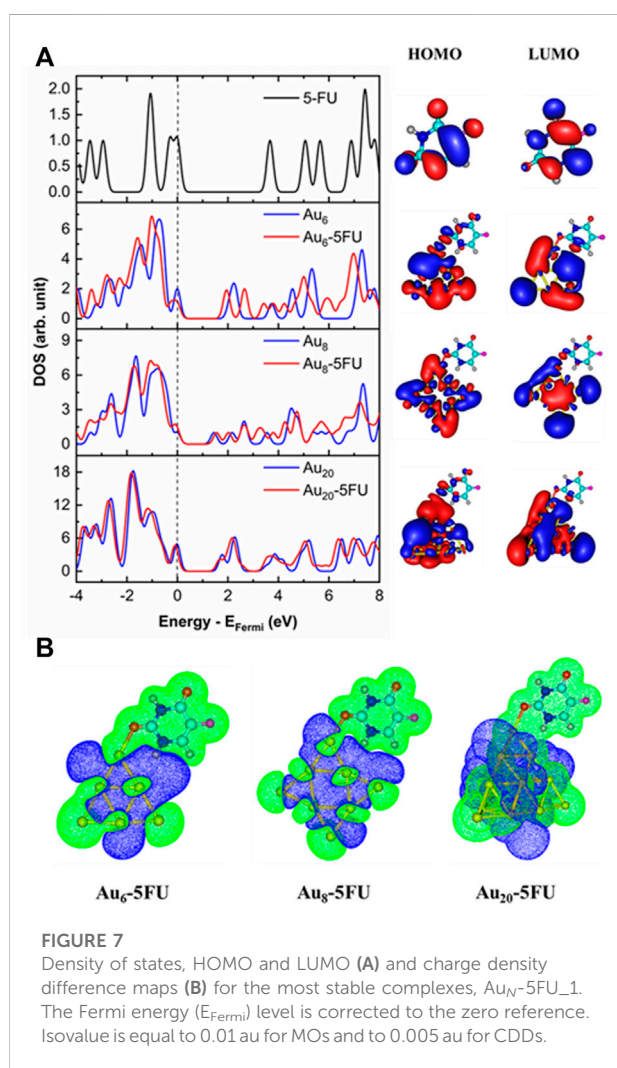
$$\Delta E_g = \frac{E_2 - E_1}{E_1} \times 100$$

where E_1 and E_2 are the band gaps in Au_N clusters and Au_N -5FU_1 complexes, respectively.

In gas-phase, the band gap of Au_8 is predicted to be 1.4 eV (Table 2), which is significantly smaller than the corresponding values of 2.1 and 1.8 eV for Au_6 and Au_{20} , respectively. The result is thus correlates well with the largest binding energy of 5FU to Au_8 cluster as analyzed above. Energies of frontier orbitals in addition provide us with important information on the binding mechanism. During the adsorption, a charge transfer could be processed from the

TABLE 2 Energies (eV) of frontier orbitals (HOMO and LUMO), their band gap (E_g) and change of E_g upon 5FU adsorption on gold clusters.

Structure	In gas phase					In water				
	HOMO	LUMO	E_F	E_g	$\% \Delta E_g$	HOMO	LUMO	E_F	E_g	$\% \Delta E_g$
5FU	-6.12	-2.44	-4.28	3.67		-5.95	-2.28	-4.12	3.67	
Au ₆	-5.94	-3.85	-4.89	2.10		-5.36	-3.07	-4.22	2.29	
Au ₆ -5FU_1	-5.68	-3.77	-4.72	1.91	-8.94	-5.24	-3.20	-4.22	2.04	-11.00
Au ₈	-5.83	-4.39	-5.11	1.44		-5.30	-3.68	-4.49	1.62	
Au ₈ -5FU_1	-5.21	-3.67	-4.44	1.54	+7.22	-5.11	-3.49	-4.30	1.61	-0.44
Au ₂₀	-5.74	-3.94	-4.84	1.79		-5.07	-3.18	-4.13	1.89	
Au ₂₀ -5FU_1	-5.63	-4.00	-4.82	1.64	-8.80	-4.99	-3.19	-4.09	1.79	-5.25



5FU molecule to the gold atoms, or reversedly depending on the energy gap between frontier states of adsorbent and adsorbate.

In the gas phase, the energy difference between the HOMO of 5FU and LUMO of gold clusters amounts to about 1.7–2.3 eV, being smaller than that involving the HOMO of gold clusters and LUMO of 5FU, which ranges from 3.3 to 3.50 eV. This leads to a decrease in the band gaps of the gold clusters after adsorption with 5FU (Figure 7A). Thus, the charge densities are mainly transferred from the HOMO of the 5FU molecule to the LUMO of a gold cluster. Such a prediction is also elucidated by the charge density difference (CDD) map analysis (Figure 7B). The CDD is computed by the following equation:

$$\Delta\rho = \rho_{complex} - \rho_{AuN} - \rho_{5FU}$$

where ρ is charge density and $\Delta\rho$ calculated by Multiwfn software. (Lu and Chen, 2012) Here, green and blue regions correspond to positive and negative regions, respectively, which also represent a decrease and an increase in electron density due to the adsorption.

A topological analysis for the most complexes Au_N-5FU₁ ($N = 6, 8, 20$) is performed and shown in Supplementary Table S1 and Supplementary Figure S1 (Supplementary File S1). The presence of bond critical points (BCPs) between Au, O and H atoms involved in intermolecular interactions in their complexes, as shown in Supplementary Figure S1, suggests that they occur. Two interactions between the gold and O, H atoms Au...O, Au...H are mainly responsible for these complex stabilization (Supplementary Figure S1). Such interactions have electron densities ρ_r that are quite low, 0.014–0.020 a.u. For Au...H and 0.049–0.053 a.u. For Au...O, indicating very weak interactions. As a result, for example Au₈-5FU₁ complex, intermolecular interaction energy (E_{int}) of these bonds around -11 kcal/mol (see in SI file). The Laplacian of electron density ($\nabla^2\rho_r$) and total electron density energy (H_r) are also important parameters for evaluating the type of non-covalent interactions (NCI). Supplementary Tables S1 shown the $\nabla^2\rho_r < 0$ and $H_r < 0$, this confirmed to be partially covalent character. Finally the reduced density gradient (RDG) which is also an efficient method for analyzing the NCI, are described in the SI file.

The energy decomposition analysis (EDA) is considered as an effective method for a quantitative interpretation of chemical bonding in terms of three main components (Morokuma, 1971; Ziegler and Rauk, 1977; Zhao et al., 2018). Accordingly, the instantaneous interaction energy ΔE_{int} between two fragments A and B in a molecule A–B is partitioned in three terms including 1) the quasi-classical electrostatic interaction ΔE_{elstat} between the fragments; 2) the repulsive exchange (Pauli) interaction ΔE_{Pauli} between electrons of the two fragments having the same spin, and 3) the orbital (covalent) interaction ΔE_{orb} which comes from the orbital relaxation and the orbital mixing between the fragments. The latter term can be decomposed into contributions from orbitals with different symmetry which make it possible to distinguish between σ , π , and δ bonding. Thus, ΔE_{int} is calculated according to the following expression (Liu, 2007):

$$\Delta E_{\text{int}} = \Delta E_{\text{elstat}} + \Delta E_{\text{Pauli}} + \Delta E_{\text{orb}} = \Delta E_{\text{steric}} + \Delta E_{\text{orb}}$$

Our EDA analysis results are performed using Multiwfn software (Lu and Chen, 2012). For example, the interaction energy of Au₈-5FU complex is -24 kcal/mol. The orbital interaction energy -41 kcal/mol significantly stabilizes the product; while the steric term (sum of electrostatic interaction energy, Pauli repulsion energy and change in exchange-correlation energy), destabilizes the adduct by 17 kcal/mol (see Supplementary Table S2 in SI file).

SERS spectra of 5FU on gold surfaces

Analyses of the vibrational signatures and the surface-enhanced Raman scattering (SERS) spectra are the effective tools for the rationalization of the drug binding mechanism on nanoparticles surfaces. In principle, Raman spectroscopy allows us to detect vibrational features of functional groups in organic compounds. However, when molecules are present at very low concentrations, this technique is naturally restricted due to the intrinsically weak Raman intensity. In this situation, the Raman intensities are often magnified by the use of the SERS techniques (Mohammadi et al., 2018). In order to interpret the SERS phenomenon, both chemical and electromagnetic enhancement mechanisms are frequently taken into accounts (Farquharson et al., 2008). A number of theoretical and experimental studies on the Raman and SERS spectra of 5FU molecule have been carried out (Farquharson et al., 2005; Cialla et al., 2014). In the present study, both Raman and SERS spectra of the 5FU molecule and its complexes in the range of 400–3600 cm⁻¹ are simulated and illustrated in Figure 8, while details of some significant signals are provided in Table 3. The experimental data for free 5FU are also included in Table 3 for a comparison.

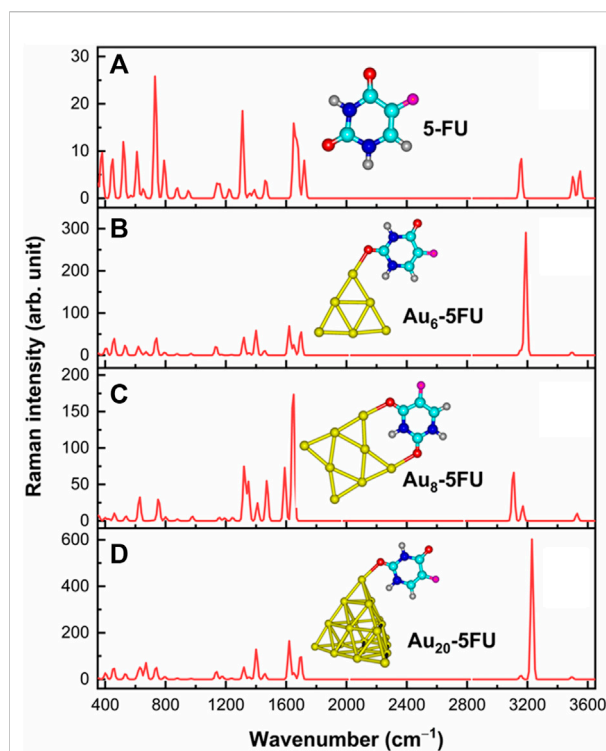


FIGURE 8
Raman signatures of 5FU (A) and its SERS spectra on Au_N (N = 6, 8, 20) surfaces (B–D) in aqueous solution.

The Raman spectrum of 5FU is basically characterized by typical signals in the regions of 400–800, 1000–1800 and 3000–3600 cm⁻¹. Several peaks located above 3000 cm⁻¹ are due to the $\nu(\text{C-H})$, $\nu(\text{N1-H})$ and $\nu(\text{N3-H})$ stretching modes. In particular, the calculated $\nu(\text{C-H})$ stretching at 3156 cm⁻¹ can be assigned to the experimental value of 3067 cm⁻¹ (Farquharson et al., 2008). Both $\nu(\text{N1-H})$ and $\nu(\text{N3-H})$ modes are predicted to stretch at 3547 and 3503 cm⁻¹. Because the H atom in the N3–H bond is involved in an intermolecular hydrogen bond, the wavenumber at 3503 cm⁻¹ of $\nu(\text{N3-H})$ is smaller than that of $\nu(\text{N1-H})$, which is consistent with the experimental data of 3022 (N3–H bond) and 3146 cm⁻¹ (N1–H bond) (Pavel et al., 2006). However, the calculated results of these bond stretchings are larger than the experimental counterpart (Rastogi et al., 2000).

Other important bands are related to the C=O stretching vibrations. As shown in Figure 8, these modes are observed at 1719 and 1675 cm⁻¹, which are comparable to the experimental values of 1725 cm⁻¹ and 1672 cm⁻¹ (Rastogi et al., 2000). On the contrary, the peaks centered at 1652 and 1224 cm⁻¹ that arise from the C=C and C–F stretching modes, agree well with the measured values at 1658 and 1224 cm⁻¹, respectively (Rastogi et al., 2000). In particular, the highest peak observed at 731 cm⁻¹ is due to the pyrimidine ring in-plane-deformation, and could

TABLE 3 Selected Raman frequencies (in cm^{-1}) and intensities (in arbitrary unit) for 5FU and its complexes $\text{Au}_6\text{-5FU}_1$ computed in aqueous solution.

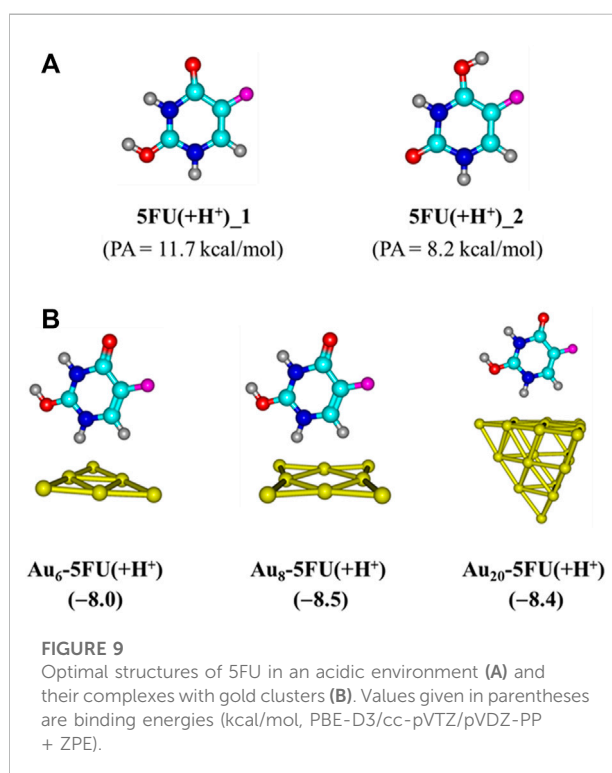
Modes*	5FU			$\text{Au}_6\text{-5FU}_1$		$\text{Au}_8\text{-5FU}_1$		$\text{Au}_{20}\text{-5FU}_1$	
	Expt	Position	Intensity	Position	Intensity	Position	Intensity	Position	Intensity
$\nu(\text{N1-H})$	3146	3548	6	3188	290	-	-	3230	602
$\nu(\text{N3-H})$	3022	3503	5	-	-	3106	56	-	-
$\nu(\text{C2=O})$	1725	1719	8	1620	69	1645	164	1700	95
$\nu(\text{C4=O})$	1672	1675	11	1697	54	1591	73	1646	160
$\beta(\text{N1-H})$	1504	1464	8	1399	58	1472	55	1398	128
$\beta(\text{C6-H})$	1258	1310	18	1318	42	1322	74	1373	60
$\delta(\text{ring})$	738	731	25	737	36	753	29	731	49

accordingly be assigned to the recorded signal at 738 cm^{-1} (Rastogi and Palafox, 2011).

Some significant variations in the SERS spectra are identified when compared with the normal Raman one as illustrated in Figures 8B–D. For example, the N1–H stretching mode in the $\text{Au}_6\text{-5FU}_1$ complex is strongly shifted to a lower energy region near 3188 cm^{-1} , as compared to a corresponding value centered at 3548 cm^{-1} in free 5FU. The C=O stretching of carbonyl groups also changes significantly. Indeed, the peaks associated with the C2 = O and C4 = O bonds are significantly shifted, in opposite directions, from 1719 to 1675 cm^{-1} in free 5FU to 1620 cm^{-1} (decreased by 99 cm^{-1}) and 1697 cm^{-1} (increased by 22 cm^{-1}) in $\text{Au}_6\text{-5FU}_1$. Other vibrations including the N1–H bending $\beta(\text{N1-H})$, C6–H bending $\beta(\text{C6-H})$ and pyrimidine ring in-plane-deformation $\delta(\text{ring})$, that are observed at 1399, 1318 and 737 cm^{-1} in $\text{Au}_6\text{-5FU}_1$. However, they are slightly changed following adsorption on gold surfaces as they are not directly involved in the interactions (Table 3). More importantly, significant modifications of the intensities are also observed. In the SERS spectra, the N–H stretching modes turn out to be the highest intensity bands, rather than the overlapped bands around 800 cm^{-1} arising from the in-plane-deformation of pyrimidine ring as in free 5FU. Such vibrations that are now centered at $3200\text{--}3400\text{ cm}^{-1}$, represent the most significant increase. Gold nanoparticles synthesized using polyethylene glycol surfactants have been used to detect several drugs such as rhodamine, 5FU and doxorubicin. It has been shown that both $\nu(\text{C=O})$ and $\beta(\text{N1-H})$ signals are significantly enhanced when coated on the gold substrate (Rastogi and Palafox, 2011).

The drug release in target cell

The drug releasing from the carrier in the target cells is one of the most important steps of a drug delivery process. In a human body, the drug can be separated from the carrier by either external or internal inducements such as the pH change or amino acid residues such as glutathione and cysteine (Rastogi



et al., 2000). As a result of an extensive lactic production, tumor cells are typically more acidic than the normal ones. Indeed, the pH of cancer cells is normally smaller than 6 as compared to values around 7.4 in blood (Swietach et al., 2014). In an acidic media, protons can attack any rich-electron site of the 5FU molecule, but it appears that the C2 = O bond emerges as the most preferred site for protonation (Figure 9A). Therefore, we now examine the effects of protons on the stability of $\text{Au}_N\text{-5FU}$ products by protonation of the C2 = O, and then carry out geometry optimizations for the resulting $\text{Au}_N\text{-5FU(+H}^+)$ complexes. As shown in Figure 9B, interactions between the 5FU molecule and gold atoms are now mainly predominated by

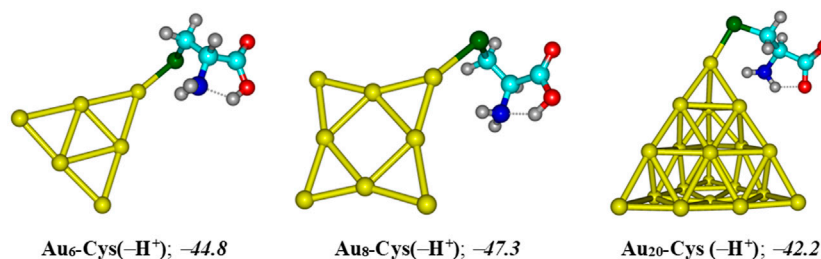
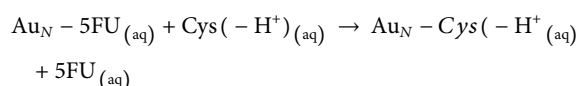


FIGURE 10

Resulting complexes of deprotonated cysteine Cys ($-\text{H}^+$) with gold clusters Au_N ($N = 6, 8, 20$). Binding energies (kcal/mol) are computed at the PBE-D3/cc-pVTZ/cc-pVDZ-PP + ZPE level.

weaker H-bonds, with a binding energy of around -8.0 kcal/mol as compared to corresponding values from -11 to -19 kcal/mol in an aqueous environment. It is expected that the 5FU drug binding to the carrier turns out to be much more breakable in an acidic environment, and thereby it is able to be released faster.

Another factor contributing crucially to drug release is an internal force related to amino acids present in the protein matrices (Ghosh et al., 2008). Some sulfur based-amino acid constituents such as cysteine and methionine are found to be the most preferred binding sites for metal particles (Ghosh et al., 2008; Swietach et al., 2014). Cysteine is a relatively strong acid with the acid dissociation constants of $\text{p}K_1 = 1.7$ and $\text{p}K_2 = 8.3$ (O'Neil, 2013). Therefore, in biological systems, it likely emerges in its deprotonated forms by a proton cleavage of either the carboxyl or thiol group (Eckhardt et al., 2013). For further insights into the drug release mechanism from the gold surfaces, we consider the following ligand exchange reaction:



The resulting complexes of Au_N clusters with the deprotonated form of cysteine, denoted as $\text{Cys}(-\text{H}^+)$, are illustrated in Figure 10. In agreement with recent reports (Nhat et al., 2020a; Si et al., 2021; Le Guével et al., 2011), these systems are mainly stabilized due to a covalent bond between the S-atom of the thiol group and the corner Au atoms. In aqueous solution, the binding energies with $\text{Cys}(-\text{H}^+)$ are predicted to be around -45 , -47 , and -42 kcal/mol for Au_6 , Au_8 and Au_{20} , respectively, that are much more negative as compared to the corresponding values obtained for a 5FU adsorption. Under neutral condition, the largest binding energies of 5FU to Au_N cluster are situated in the range of -19 to -11 kcal/mol (Table 1), but significantly reduced to -8 kcal/mol in an acidic solution (Figure 9). The results clearly indicate that the gold affinity of cysteine residues is much stronger than that of the 5FU molecule. As a result, a drug release from a gold surface is expected to be

spontaneous within the cancer cells upon protonation due to this internal inducement.

Concluding remarks

In this theoretical study we attempted to elucidate the adsorption behaviours of the 5FU cancer drug on the Au nanostructured surfaces using three small gold clusters Au_N ($N = 6, 8, 20$) as model reactants. The structures, energetics and spectroscopic properties were analyzed thoroughly by employing a functional with dispersion correction, namely the PBE-B3. The effects of solvent in an aqueous solution were also evaluated using the IEF-PCM model.

In both vacuum and aqueous solution, the 5FU molecule tends to bind with gold atoms via the oxygen atom of the $\text{C}2 = \text{O}$ group. The resulting complexes are also partially stabilized by some weak $\text{N}-\text{H}\cdots\text{Au}$ couplings. Nonetheless, in an acidic environment, the $\text{Au}\cdots\text{H}-\text{X}$ with $\text{X} = \text{O}, \text{C}$ interaction turns out to be predominant, instead of the stronger gas phase covalent $\text{Au}-\text{O}$ bond. Indeed, the largest binding energy is greatly declined from -24 kcal/mol in gas phase to -19 and -8 kcal/mol in neutral and acidic media, respectively. Following 5FU adsorption, the band gap of gold clusters is greatly modified giving rise to a significant change in the electronic properties. Analysis of the frontier MOs showed that a charge transfer from the 5FU molecule to the gold clusters constitutes the main ingredient of the 5FU–Au interaction. A mechanism for drug release from the gold surface has also been proposed and elucidated. Accordingly, such a process is triggered by either the cysteine residues present in protein matrices or the low pH in cancerous tissues.

An examination on the SERS spectra also allowed us to verify the preferable orientation of 5FU molecules on the gold surface. As being directly oriented to the gold surface, the $\text{N}-\text{H}$ stretching mode turns out to be the most dominant factor responsible for the SERS enhancement of the drug molecules. These results show that it is possible to use SERS spectroscopy to detect the 5FU molecule in an aqueous medium through the use of gold nanoparticles.

Data availability statement

The original contributions presented in the study are included in the article/**Supplementary Material**, further inquiries can be directed to the corresponding author.

Author contributions

NS carried out computations, analysed the results and wrote the first draft. PN analysed the results and edited the draft. MN supervised the work, analysed the results and finalized the manuscript.

Funding

NTS was funded by Vingroup JSC and supported by the Master, PhD Scholarship Programme of Vingroup Innovation Foundation (VinIF), Institute of Big Data, code VinIF.2021.TS.058. The authors declare that the funder was not involved in the study design, collection, analysis, interpretation of data, the writing of this article, or the decision to submit it for publication.

Acknowledgments

NS is grateful to the Mississippi Center for Supercomputer United States for computing resources.

References

- Aal, S. A. (2022). DFT study of the therapeutic potential of borospherene and metalloborospherenes as a new drug-delivery system for the 5-fluorouracil anticancer drug. *J. Mol. Liq.* 360, 119457. doi:10.1016/j.molliq.2022.119457
- Afarideh, B., Rajabibazl, M., Omid, M., Yaghmae, B., Rahimpour, A., Khodabakhshi, R., et al. (2018). Anticancer activity of graphene oxide/5-FU on CT26 Ds-Red adenocarcinoma cell line. *Orient. J. Chem.* 34 (4), 2002–2007. doi:10.13005/ojc/3404038
- Al-Jumayli, M., Choucair, K., Al-Obaidi, A., Park, R., Bansal, A., Baranda, J., et al. (2022). Pre-operative carboplatin/paclitaxel versus 5-fluorouracil (5-fu)-based chemoradiotherapy for older adults with esophageal cancer. *Anticancer Res.* 42 (1), 59–66. doi:10.21873/anticancer.15457
- Al-Musawi, S., Hadi, A. J., Hadi, S. J., and Hindi, N. K. K. (2019). Preparation and characterization of folated chitosan-magnetic nanocarrier for 5-fluorouracil drug delivery and studying its effect in bladder cancer therapy. *J. Glob. Pharm. Technol.* 11, 628–637.
- Bai, X., Wang, Y., Song, Z., Feng, Y., Chen, Y., Zhang, D., et al. (2020). The basic properties of gold nanoparticles and their applications in tumor diagnosis and treatment. *Int. J. Mol. Sci.* 21 (7), 2480. doi:10.3390/ijms21072480
- Bansal, S. A., Kumar, V., Karimi, J., Singh, A. P., and Kumar, S. (2020). Role of gold nanoparticles in advanced biomedical applications. *Nanoscale Adv.* 2 (9), 3764–3787. doi:10.1039/d0na00472c
- Chen, F., Si, P., de la Zerda, A., Jokerst, J. V., and Myung, D. (2021). Gold nanoparticles to enhance ophthalmic imaging. *Biomater. Sci.* 9 (2), 367–390. doi:10.1039/d0bm01063d
- Chen, J., Qiu, M., Zhang, S., Li, B., Li, D., Huang, X., et al. (2022). A calcium phosphate drug carrier loading with 5-fluorouracil achieving a synergistic effect for pancreatic cancer therapy. *J. Colloid Interface Sci.* 605, 263–273. doi:10.1016/j.jcis.2021.07.080
- Cialla, D., Pollok, S., Steinbrücker, C., Weber, K., and Popp, J. (2014). SERS-based detection of biomolecules. *Nanophotonics* 3 (6), 383–411. doi:10.1515/nanoph-2013-0024
- de Oliveira, B. E., Amorim, O. H. J., Lima, L. L., Rezende, R. A., Mestnik, N. C., Bagatin, E., et al. (2021). 5-Fluorouracil, innovative drug delivery systems to enhance bioavailability for topical use. *J. Drug Deliv. Sci. Technol.* 61, 102155. doi:10.1016/j.jddst.2020.102155
- Dos Santos, A. M., Junior, A. G. T., Carvalho, S. G., and Chorilli, M. (2022). An updated review on properties, nanodelivery systems, and analytical methods for the determination of 5-fluorouracil in pharmaceutical and biological samples. *Curr. Pharm. Des.* 28, 1501–1512. doi:10.2174/1381612828666220509150918
- Du, Y., Xia, L., Jo, A., Davis, R. M., Bissel, P., Ehrlich, M. F., et al. (2018). Synthesis and evaluation of doxorubicin-loaded gold nanoparticles for tumor-targeted drug delivery. *Bioconjugate Chem.* 29 (2), 420–430. doi:10.1021/acs.bioconjchem.7b00756
- Eckhardt, S., Brunetto, P. S., Gagnon, J., Priebe, M., Giese, B., and Fromm, K. M. (2013). Nanobio silver: Its interactions with peptides and bacteria, and its uses in medicine. *Chem. Rev.* 113 (7), 4708–4754. doi:10.1021/cr300288v
- Elahi, N., Kamali, M., and Baghersad, M. H. (2018). Recent biomedical applications of gold nanoparticles: A review. *Talanta* 184, 537–556. doi:10.1016/j.talanta.2018.02.088
- Farquharson, S., Gift, A., Shende, C., Inscore, F., Ordway, B., Farquharson, C., et al. (2008). Surface-enhanced Raman spectral measurements of 5-fluorouracil in saliva. *Molecules* 13 (10), 2608–2627. doi:10.3390/molecules13102608
- Farquharson, S., Shende, C., Inscore, F. E., Maksymjuk, P., and Gift, A. (2005). Analysis of 5-fluorouracil in saliva using surface-enhanced Raman spectroscopy. *J. Raman Spectrosc.* 36 (3), 208–212. doi:10.1002/jrs.1277

MN thanks KU Leuven Belgium for support for open access publication, and is thankful to Van Lang University, Vietnam.

Conflict of interest

The authors declare that the research was conducted in the absence of any commercial or financial relationships that could be construed as a potential conflict of interest.

Publisher's note

All claims expressed in this article are solely those of the authors and do not necessarily represent those of their affiliated organizations, or those of the publisher, the editors and the reviewers. Any product that may be evaluated in this article, or claim that may be made by its manufacturer, is not guaranteed or endorsed by the publisher.

Supplementary material

The Supplementary Material for this article can be found online at: <https://www.frontiersin.org/articles/10.3389/fchem.2022.1050423/full#supplementary-material>

- Franquet-Griell, H., Gómez-Canela, C., Ventura, F., and Lacorte, S. (2015). Predicting concentrations of cytostatic drugs in sewage effluents and surface waters of Catalonia (NE Spain). *Environ. Res.* 138, 161–172. doi:10.1016/j.envres.2015.02.015
- Freitas de Freitas, L., Varca, G. H. C., dos Santos Batista, J. G., and Benévolo Lugo, A. (2018). An overview of the synthesis of gold nanoparticles using radiation technologies. *Nanomaterials* 8 (11), 939. doi:10.3390/nano8110939
- Frisch, M. J., Trucks, G. W., Schlegel, H. B., Scuseria, G. E., Robb, M. A., Cheeseman, J. R., et al. (2019). *Gaussian 16, rev. C.01*. Wallingford CT: Gaussian, Inc.
- Frydenberg, H., Harsem, N. K., Ofigsbø, Å., Skoglund, H., Brændengen, M., Kaasa, S., et al. (2020). Chemotherapy during pregnancy for advanced colon cancer: A case report. *Clin. Colorectal Cancer* 19 (2), 141–144. doi:10.1016/j.clcc.2020.02.013
- Ghosh, P., Han, G., De, M., Kim, C. K., and Rotello, V. M. (2008). Gold nanoparticles in delivery applications. *Adv. Drug Deliv. Rev.* 60 (11), 1307–1315. doi:10.1016/j.addr.2008.03.016
- Grimme, S., Antony, J., Ehrlich, S., and Krieg, H. (2010). Fundamentals of time-dependent density functional theory. *J. Chem. Phys.* 132, 1541041–15410419.
- Gui, R., Wan, A., and Jin, H. (2013). Retracted Article: Facile synthesis of quantum dots/mesoporous silica/quantum dots core/shell/shell hybrid microspheres for ratiometric fluorescence detection of 5-fluorouracil in human serum. *Analyst* 138 (20), 5956–5964. doi:10.1039/c3an01089a
- Hadipour, N. L., Ahmadi Peyghan, A., and Soleymanabadi, H. (2015). Theoretical study on the Al-doped ZnO nanoclusters for CO chemical sensors. *J. Phys. Chem. C* 119 (11), 6398–6404. doi:10.1021/jp513019z
- Hang, N. T. N., Si, N. T., Nguyen, M. T., and Nhat, P. V. (2021). Adsorption/desorption behaviors and SERS chemical enhancement of 6-mercaptopurine on a nanostructured gold surface: The Au₂₀ cluster model. *Molecules* 26 (17), 5422. doi:10.3390/molecules26175422
- Hanif, M., Akhtar, M. F., Naeem, S., Wahid, M., Shehzad, M. A., Saadullah, M., et al. (2018). Development and validation of a new HPLC method for the detection of 5-fluorouracil in mobile phase and in plasma. *Curr. Pharm. Anal.* 14 (1), 3–7. doi:10.2174/1573412912666160922124552
- Horo, H., Das, S., Mandal, B., and Kundu, L. M. (2019). Development of a photoresponsive chitosan conjugated prodrug nano-carrier for controlled delivery of antitumor drug 5-fluorouracil. *Int. J. Biol. Macromol.* 121, 1070–1076. doi:10.1016/j.ijbiomac.2018.10.095
- Ibrahim, R. A. A.-Z., Al-Hakeim, H. K., and Suhail, F. S. A. (2018). Anticancer drug 5-Fluorouracil in aqueous solution by differential pulse polarography: An assessment of optimum conditions. *Nano Biomed. Eng.* 10 (2), 117–128. doi:10.5101/nbe.v10i2.p117-128
- James, A. M., and Lord, M. P. (1992). *Macmillan's chemical and physical data*. London, United Kingdom: Macmillan.
- Kaur, J., Gill, G. S., and Jeet, K. (2019). "Applications of carbon nanotubes in drug delivery: A comprehensive review," in *Characterization and biology of nanomaterials for drug delivery* (Amsterdam, Netherlands: Elsevier), 113–135.
- Khodarahmi, M., Abbasi, H., Kouchak, M., Mahdavinia, M., Handali, S., and Rahbar, N. (2022). Nanoencapsulation of aptamer-functionalized 5-Fluorouracil liposomes using alginate/chitosan complex as a novel targeting strategy for colon-specific drug delivery. *J. Drug Deliv. Sci. Technol.* 71, 103299. doi:10.1016/j.jddst.2022.103299
- Khoshnevisan, K., Daneshpour, M., Barkhi, M., Gholami, M., Samadian, H., and Maleki, H. (2018). The promising potentials of capped gold nanoparticles for drug delivery systems. *J. Drug Target.* 26 (7), 525–532. doi:10.1080/1061186x.2017.1387790
- Kryachko, E., and Remacle, F. (2005). Three-gold clusters form nonconventional hydrogen bonds O–H... Au and N–H... Au with formamide and formic acid. *Chem. Phys. Lett.* 404 (1–3), 142–149. doi:10.1016/j.cplett.2005.01.061
- Le Guével, X., Hötzer, B., Jung, G., Hollemeyer, K., Trouillet, V., and Schneider, M. (2011). Formation of fluorescent metal (Au, Ag) nanoclusters capped in bovine serum albumin followed by fluorescence and spectroscopy. *J. Phys. Chem. C* 115 (22), 10955–10963. doi:10.1021/jp111820b
- Lee, K. X., Shameli, K., Yew, Y. P., Teow, S.-Y., Jahangirian, H., Rafiee-Moghaddam, R., et al. (2020). Recent developments in the facile biosynthesis of gold nanoparticles (AuNPs) and their biomedical applications. *Int. J. Nanomedicine* 15, 275–300. doi:10.2147/ijn.s233789
- Li, J., Lu, F., Shao, X., and You, B. (2021). 5-FU@ DHA-UIO-66-NH₂ potentiates chemotherapy sensitivity of breast cancer cells through a microRNA let-7a-dependent mechanism. *Ann. Transl. Med.* 9, 1761. doi:10.21037/atm-21-5978
- Li, Q., Wang, J., Ding, Q., Chen, M., and Ma, F. (2017). Coupling effect on charge-transfer mechanism of surface-enhanced resonance Raman scattering. *J. Raman Spectrosc.* 48 (4), 560–569. doi:10.1002/jrs.5077
- Liu, H., He, Y., and Cao, K. (2021). Flexible surface-enhanced Raman scattering substrates: A review on constructions, applications, and challenges. *Adv. Mat. Interfaces* 8 (21), 2100982. doi:10.1002/admi.202100982
- Liu, L., Anwar, S., Ding, H., Xu, M., Yin, Q., Xiao, Y., et al. (2019). Electrochemical sensor based on F, N-doped carbon dots decorated laccase for detection of catechol. *J. Electroanal. Chem.* 840, 84–92. doi:10.1016/j.jelechem.2019.03.071
- Liu, S. (2007). Steric effect: A quantitative description from density functional theory. *J. Chem. Phys.* 126 (24), 244103. doi:10.1063/1.2747247
- Lu, T., and Chen, F. (2012). Multiwfn: A multifunctional wavefunction analyzer. *J. Comput. Chem.* 33 (5), 580–592. doi:10.1002/jcc.22885
- Manzano, M., and Vallet-Regí, M. (2020). Mesoporous silica nanoparticles for drug delivery. *Adv. Funct. Mat.* 30 (2), 1902634. doi:10.1002/adfm.201902634
- Markova, N., Enchev, V., and Ivanova, G. (2010). Tautomeric equilibria of 5-fluorouracil anionic species in water. *J. Phys. Chem. A* 114 (50), 13154–13162. doi:10.1021/jp1063879
- Mazzuca, F., Borro, M., Botticelli, A., Mazzotti, E., Marchetti, L., Gentile, G., et al. (2016). Pre-treatment evaluation of 5-fluorouracil degradation rate: Association of poor and ultra-rapid metabolism with severe toxicity in a colorectal cancer patients cohort. *Oncotarget* 7 (15), 20612–20620. doi:10.18632/oncotarget.7991
- Minhas, M. U., Abdullah, O., Sohail, M., Khalid, I., Ahmad, S., Khan, K. U., et al. (2021). Synthesis of novel combinatorial drug delivery system (nCDDS) for co-delivery of 5-fluorouracil and leucovorin calcium for colon targeting and controlled drug release. *Drug Dev. Industrial Pharm.* 47 (12), 1952–1965. doi:10.1080/03639045.2022.2072514
- Mirhaji, E., Afshar, M., Rezvani, S., and Yoosefian, M. (2018). Boron nitride nanotubes as a nanotransporter for anti-cancer docetaxel drug in water/ethanol solution. *J. Mol. Liq.* 271, 151–156. doi:10.1016/j.molliq.2018.08.142
- Mohammadi, A., Nicholls, D. L., and Docoslis, A. (2018). Improving the surface-enhanced Raman scattering performance of silver nanodendritic substrates with sprayed-on graphene-based coatings. *Sensors* 18 (10), 3404. doi:10.3390/s18103404
- Morokuma, K. (1971). Molecular orbital studies of hydrogen bonds. III. C=O...H–O hydrogen bond in H₂CO...H₂O and H₂CO...2H₂O. *J. Chem. Phys.* 55 (3), 1236–1244. doi:10.1063/1.1676210
- Mullot, J.-U., Karolak, S., Fontova, A., Huart, B., and Levi, Y. (2009). Development and validation of a sensitive and selective method using GC/MS-MS for quantification of 5-fluorouracil in hospital wastewater. *Anal. Bioanal. Chem.* 394 (8), 2203–2212. doi:10.1007/s00216-009-2902-x
- Nguyen, C.-H., Banh, K.-S., Dang, C.-H., Nguyen, C.-H., and Nguyen, T.-D. (2022). β -cyclodextrin/alginate nanoparticles encapsulated 5-fluorouracil as an effective and safe anticancer drug delivery system. *Arabian J. Chem.* 15 (6), 103814. doi:10.1016/j.arabj.2022.103814
- Nhat, P. V., Nguyen, P. T. N., and Si, N. T. (2020). A computational study of thiol-containing cysteine amino acid binding to Au₆ and Au₈ gold clusters. *J. Mol. Model.* 26 (3), 58. doi:10.1007/s00894-020-4312-0
- Nhat, P. V., Si, N. T., Leszczynski, J., and Nguyen, M. T. (2017). Another look at structure of gold clusters Au_n from perspective of phenomenological shell model. *Chem. Phys.* 493, 140–148. doi:10.1016/j.chemphys.2017.06.009
- Nhat, P. V., Si, N. T., Tram, N. T. T., Duong, L. V., and Nguyen, M. T. (2020). Elucidating the binding mechanism of thione-containing mercaptopurine and thioguanine drugs to small gold clusters. *J. Comput. Chem.* 41 (19), 1748–1758. doi:10.1002/jcc.26216
- Nițiță, Ș., Moldovan, A. I., Toma, V., Moldovan, C. S., Berindan-Neagoe, I., Știufiuc, G., et al. (2018). PEGylated gold nanoparticles with interesting plasmonic properties synthesized using an original, rapid, and easy-to-implement procedure. *J. Nanomater.* 2018, 1–7. doi:10.1155/2018/5954028
- O'boyle, N. M., Tenderholt, A. L., and cclib, Langner K. M. (2008). cclib: A library for package-independent computational chemistry algorithms. *J. Comput. Chem.* 29 (5), 839–845. doi:10.1002/jcc.20823
- O'Neil, M. J. (2013). *The merck index: An encyclopedia of chemicals, drugs, and biologicals*. London, United Kingdom: RSC Publishing.
- Oliveira, M. M. B., de Araújo, A. A., Ribeiro, S. B., de Sales Mota, P. C. M., Marques, V. B., da Silva Martins Rebouças, C., et al. (2021). Losartan improves intestinal mucositis induced by 5-fluorouracil in mice. *Sci. Rep.* 11 (1), 23241–23312. doi:10.1038/s41598-021-01969-x
- Onishi, H., Nagai, T., and Machida, Y. (2020). *Applications of chitin, chitosan, and their derivatives to drug carriers for microparticulated or conjugated drug delivery systems. Applications of chitin and chitosan*. Florida, United States: CRC Press, 205–231.
- Pakiari, A., and Jamshidi, Z. (2007). Interaction of amino acids with gold and silver clusters. *J. Phys. Chem. A* 111 (20), 4391–4396. doi:10.1021/jp070306t

- Pascu, M. L., Brezeanu, M., Voicu, L., Staicu, A., Carstocea, B., and Pascu, R. A. (2005). 5-fluorouracil as a photosensitizer. *Vivo* 19 (1), 215–220.
- Pavel, I., Cota, S., Kiefer, W., and Cintiă-Pinzaru, S. (2006). SERS substrate-dependent interaction of the anticarcinogenic drug 5-fluorouracil with silver. *Part. Sci. Technol.* 24 (3), 301–309. doi:10.1080/02726350600840639
- Perdew, J. P., Burke, K., and Ernzerhof, M. (1996). Generalized gradient approximation made simple. *Phys. Rev. Lett.* 77 (18), 3865–3868. doi:10.1103/physrevlett.77.3865
- Peterson, K. A. (2003). Systematically convergent basis sets with relativistic pseudo-potentials. I. Correlation consistent basis sets for the post-d group 13–15 elements. *J. Chem. Phys.* 119 (21), 11099–11112. doi:10.1063/1.1622923
- Rastogi, V., Jain, V., Yadav, R., Singh, C., and Palafox, M. A. (2000). Fourier transform Raman spectrum and *ab initio* and density functional computations of the vibrational spectrum, molecular geometry, atomic charges and some molecular properties of the anticarcinogenic drug 5-fluorouracil. *J. Raman Spectrosc.* 31 (7), 595–603. doi:10.1002/1097-4555(200007)31:7<595::aid-jrs582>3.0.co;2-9
- Rastogi, V., and Palafox, M. A. (2011). Vibrational spectra, tautomerism and thermodynamics of anticarcinogenic drug: 5-Fluorouracil. *Spectrochimica Acta Part A Mol. Biomol. Spectrosc.* 79 (5), 970–977. doi:10.1016/j.saa.2011.04.008
- Román, G., Nosedá Grau, E., Brizuela, G., Juan, A., and Simonetti, S. (2018). A first-principles study of pristine and Al-doped activated carbon interacting with 5-Fluorouracil anticancer drug. *Eur. Phys. J. E* 41 (9), 107–116. doi:10.1140/epje/i2018-11718-4
- Rowney, N. C., Johnson, A. C., and Williams, R. J. (2009). Cytotoxic drugs in drinking water: A prediction and risk assessment exercise for the Thames catchment in the United Kingdom. *Environ. Toxicol. Chem.* 28 (12), 2733–2743. doi:10.1897/09-067.1
- Sanad, M. F., Shalan, A. E., Bazid, S. M., Serea, E. S. A., Hashem, E. M., Nabih, S., et al. (2019). A graphene gold nanocomposite-based 5-FU drug and the enhancement of the MCF-7 cell line treatment. *RSC Adv.* 9 (53), 31021–31029. doi:10.1039/c9ra05669f
- Sargazi-Avval, H., Yoosefian, M., Ghaffari-Moghaddam, M., Khajeh, M., and Bohlooli, M. (2021). Potential applications of armchair, zigzag, and chiral boron nitride nanotubes as a drug delivery system: Letrozole anticancer drug encapsulation. *Appl. Phys. A* 127 (4), 257–7. doi:10.1007/s00339-021-04402-2
- Scanlan, M. J., and Hillier, I. H. (1984). An *ab initio* study of tautomerism of uracil, thymine, 5-fluorouracil, and cytosine. *J. Am. Chem. Soc.* 106 (13), 3737–3745. doi:10.1021/ja00325a005
- Schlücker, S. (2014). Surface-Enhanced Raman spectroscopy: Concepts and chemical applications. *Angew. Chem. Int. Ed.* 53 (19), 4756–4795. doi:10.1002/anie.201205748
- Shakerzadeh, E., Zborowski, K. K., Anota, E. C., and Nguyen, M. T. (2022). Pristine and alkali and alkaline Earth metals encapsulated B36N36 nanoclusters as prospective delivery agents and detectors for 5-fluorouracil anticancer drug. *Appl. Organomet. Chem.* 36 (7), e6721. doi:10.1002/aoc.6721
- Si, N. T., Nhung, N. T. A., Bui, T. Q., Nguyen, M. T., and Nhat, P. V. (2021). Gold nanoclusters as prospective carriers and detectors of pramipexole. *RSC Adv.* 11 (27), 16619–16632. doi:10.1039/d1ra02172a
- Siddique, S., and Chow, J. C. (2020). Gold nanoparticles for drug delivery and cancer therapy. *Appl. Sci.* 10 (11), 3824. doi:10.3390/app10113824
- Solhjo, A., Sobhani, Z., Sufali, A., Rezaei, Z., Khabnadideh, S., and Sakhteman, A. (2021). Exploring pH dependent delivery of 5-fluorouracil from functionalized multi-walled carbon nanotubes. *Colloids Surfaces B Biointerfaces* 205, 111823. doi:10.1016/j.colsurfb.2021.111823
- Sotnikov, D. V., Berlina, A. N., Ivanov, V. S., Zherdev, A. V., and Dzantiev, B. B. (2019). Adsorption of proteins on gold nanoparticles: One or more layers? *Colloids Surfaces B Biointerfaces* 173, 557–563. doi:10.1016/j.colsurfb.2018.10.025
- Swietach, P., Vaughan-Jones, R. D., Harris, A. L., and Hulikova, A. (2014). The chemistry, physiology and pathology of pH in cancer. *Phil. Trans. R. Soc. B* 369 (1638), 20130099. doi:10.1098/rstb.2013.0099
- Taghizadeh, S., Alimardani, V., Roudbali, P. L., Ghasemi, Y., and Kaviani, E. (2019). Gold nanoparticles application in liver cancer. *Photodiagnosis Photodyn. Ther.* 25, 389–400. doi:10.1016/j.pdpdt.2019.01.027
- Tendwa, M. B., Chebon-Bore, L., Lobb, K., Musyoka, T. M., and Bishop Ö, T. (2021). Force field parameters for Fe²⁺/S²⁻ clusters of dihydropyrimidine dehydrogenase, the 5-fluorouracil cancer drug deactivation protein: A step towards *in silico* pharmacogenomics studies. *Molecules* 26 (10), 2929. doi:10.3390/molecules26102929
- Tomasi, J., Mennucci, B., and Cammi, R. (2005). Quantum mechanical continuum solvation models. *Chem. Rev.* 105 (8), 2999–3094. doi:10.1021/cr9904009
- Vodenkova, S., Buchler, T., Cervena, K., Veskrnova, V., Vodicka, P., and Vymetalkova, V. (2020). 5-fluorouracil and other fluoropyrimidines in colorectal cancer: Past, present and future. *Pharmacol. Ther.* 206, 107447. doi:10.1016/j.pharmthera.2019.107447
- Wang, C., Shen, L., and Wu, L. (2021). Adsorption and sensing of an anticancer drug on the boron nitride nanotubes; a computational inspection. *Comput. Methods Biomechanics Biomed. Eng.* 24 (2), 151–160. doi:10.1080/10255842.2020.1815716
- Weiss, A., and Haran, G. (2001). Time-dependent single-molecule Raman scattering as a probe of surface dynamics. *J. Phys. Chem. B* 105 (49), 12348–12354. doi:10.1021/jp0126863
- Wielnińska, J., Nowacki, A., and Liberek, B. (2019). 5-fluorouracil—Complete insight into its neutral and ionised forms. *Molecules* 24 (20), 3683. doi:10.3390/molecules24203683
- Yuksel, N., Kose, A., and Fellah, M. F. (2022). A Density Functional Theory study for adsorption and sensing of 5-Fluorouracil on Ni-doped boron nitride nanotube. *Mater. Sci. Semicond. Process.* 137, 106183. doi:10.1016/j.mssp.2021.106183
- Zahed, F. M., Hatamluyi, B., Lorestani, F., and Es'haghi, Z. (2018). Silver nanoparticles decorated polyaniline nanocomposite based electrochemical sensor for the determination of anticancer drug 5-fluorouracil. *J. Pharm. Biomed. Analysis* 161, 12–19. doi:10.1016/j.jpba.2018.08.004
- Zarghami Dehaghani, M., Yousefi, F., Sajadi, S. M., Tajammal Munir, M., Abida, O., Habibzadeh, S., et al. (2021). Theoretical encapsulation of fluorouracil (5-fu) anti-cancer chemotherapy drug into carbon nanotubes (cnt) and boron nitride nanotubes (bnnt). *Molecules* 26 (16), 4920. doi:10.3390/molecules26164920
- Zhang, L., Mazouzi, Y., Salmain, M., Liedberg, B., and Boujday, S. (2020). Antibody-gold nanoparticle bioconjugates for biosensors: Synthesis, characterization and selected applications. *Biosens. Bioelectron.* 165, 112370. doi:10.1016/j.bios.2020.112370
- Zhao, L., von Hopffgarten, M., Andrada, D. M., and Frenking, G. (2018). Energy decomposition analysis. *WIREs Comput. Mol. Sci.* 8 (3), e1345. doi:10.1002/wcms.1345
- Ziegler, T., and Rauk, A. (1977). On the calculation of bonding energies by the Hartree Fock Slater method. *Theor. Chim. Acta* 46 (1), 1–10. doi:10.1007/bf02401406